Research Article

BIOMEDICAL Journal of Scientific & Technical Research

ISSN: 2574 -1241

DOI: 10.26717/BJSTR.2023.53.008398

Calcium Buffering by Fluorescent Indicators – Implications and Easy Solutions

Krzysztof L Hyrc[1,4]*, Ziemowit Rzeszotnik[2], Mark P Goldberg[3#] and Colin G Nichols[4#]

[1]*The Hope Center for Neurological Disorders, Alafi Neuroimaging Laboratory and Department of Neurology, Washington University School of Medicine, USA*

[2]*Institute of Mathematics, Wroclaw University, Poland*

[3]*Department of Neurology and Neurotherapeutics, University of Texas Southwestern Medical Center, USA*

[4]*Center for Investigations of Membrane Excitability Diseases, Washington University, School of Medicine, USA*

[#]*These authors are contributed equally*

***Corresponding author:** Krzysztof L Hyrc, Washington University School of Medicine,Department of Neurology (Campus Box 8111)660 S. Euclid Ave, Saint Louis, USA

ARTICLE INFO

Received: October 12, 2023

Published: October 20, 2023

Citation: Krzysztof L Hyrc, Ziemowit Rzeszotnik, Mark P Goldberg and Colin G Nichols. Calcium Buffering by Fluorescent Indicators – Implications and Easy Solutions. Biomed J Sci & Tech Res 53(3)-2023. BJSTR. MS.ID.008398.

ABSTRACT

Intracellular free calcium concentrations ($[Ca^{2+}]_i$) are commonly measured with fluorescent indicators. As Ca^{2+} chelators, they compete with endogenous buffers for Ca^{2+} ions, which may reduce $[Ca^{2+}]_i$. Indicator concentrations that are unlikely to markedly affect Ca^{2+} signals were defined long time ago, but they are usually too low to allow accurate fluorescence measurements. In consequence, most routine $[Ca^{2+}]_i$ measurements utilize much higher indicator concentrations and may underestimate $[Ca^{2+}]_i$. Here, we propose a method to derive correct, indicator-independent) $[Ca^{2+}]_i$ by extrapolating the reported $[Ca^{2+}]_i$ to the indicator-free environment. Although similar to its predecessors, the proposed steady-state model avoids complexities of earlier approaches and requires only data collected in AM ester loaded cells. As such, it can be applied to determine the indicator-independent peak $[Ca^{2+}]_i$ induced by any stimulus in any cell type. First, we tested the approach in well-defined in vitro systems and found that it determined the indicator-independent Ca^{2+} quite well and estimated albeit less accurately concentration and affinity of an endogenous buffer. When applied to the data collected in fura-2 loaded neurons depolarized with 50 mM K+, the method estimated the true Ca^{2+} in resting (22 nM) and stimulated (1.18 μM) neurons and characterized the endogenous buffer (~600 μM) as having low affinity ($0.78 \leq K_b \leq 1.63$ μM), values resembling those determined previously. While the method does not account for indicator-distorted Ca^{2+}decay rates (a consequence of omitting the time component), it creates a simple way to assess peak Ca^{2+} amplitudes, the values most often desired in routine Ca^{2+}imaging experiments.

Keywords: Intracellular Calcium; Fluorescent Indicators; Neurons; Fura-2; Endogenous Buffers; Mathematical Modelling

Abbreviations: Cat: Total Calcium Concentration; caf_o and caf_{free}: Free Calcium Concentration in the Absence (native) and Presence of an Exogenous Buffer (an Indicator); Ion, Buf and Dye: Total Concentration of Ions, Endogenous Buffer and Exogenous Buffer (Indicator); Ion_o, and Buf_o– Native Ion and Intrinsic Buffer Concentrations in the Absence of an Indicator; Ion_{free}, and Buf_{free}: Free Ion and Intrinsic Buffer Concentrations in the Presence of an Indicator; Buf_{Ca}, an Dye_{Ca}: Concentrations of Calcium-Bound Duffer and Indicator; K_d and K_b - Indicator and Buffer Dissociation Constants; κ_S and κ_d -Cytoplasm and Indicator Calcium Binding Ratio Defined Precisely in Text and Previous Publications

Introduction

The determination of cytosolic free calcium concentration ($[Ca^{2+}]_i$) an important secondary messenger [1-4], is typically accomplished with the use of fluorescent indicators [5-8]. Varying widely with respect to their spectral and binding properties [9-12], indicators share common design and operation principles. A typical indicator molecule comprises a calcium binding moiety, usually BAPTA [13] or a derivative [9], linked to a fluorophore, such as stilbene [14], fluorescein or rhodamine [15]. While the former determines indicator affinity and selectivity, the latter defines its spectral properties. The binding of Ca^{2+} ions by BAPTA changes electron distribution within the molecule, which in turn leads to a fluorescence change, which may involve a shift in excitation or emission wavelength [14,16]. In every case, the indicator must first bind Ca^{2+} and therefore inevitably acts as a calcium buffer (for recent reviews see [17,18]). The number of sequestered ions depends on indicator affinity and concentration. For the sake of simplicity, only the former is considered by the standard equation commonly used to convert indicator signal into $[Ca^{2+}]_i$ [14]. Omitting the indicator concentration may be inconsequential in calibration solutions containing large amounts of calcium and EGTA (1-10 mM) whose proportion sets the free $[Ca^{2+}]$ (0-40 μM) [19,20], a balance practically unchanged by adding indicator at low concentrations (≤5 μM) in *in vitro* measurements.

The situation in in situ experiments however might be quite different. Not only is the buffering capacity of the cytosol much lower than in millimolar EGTA [21-26], but the cytosolic indicator concentrations tend to be much higher (30-150 μM [27-33]) than those used *in vitro*. While such high concentrations might be required to ensure high signal to noise ratio [34,35], the indicator may bind a substantial fraction of Ca^{2+} ions and lower their free concentration, in consequence, reporting a lower $[Ca^{2+}]_i$ that is affected by indicator concentration and affinity [36-40].This problem was recognized in early studies demonstrating that higher indicator concentrations produced lower $[Ca^{2+}]_i$ estimates [41-44]. Similarly, low affinity indicators were often found to report higher $[Ca^{2+}]$ values than their high affinity analogues. For example, fura-2 (K_d ~0.22 μM [14]) was shown to report higher Ca^{2+} transients [45-47] than quin-2 (K_d=0.115 μM [27]). Ito and coworkers observed marked differences in $[Ca^{2+}]_i$ measured using fura-2 and BTC[48] (K_d ~12 μM [49]) in pancreatic acinar cells [50]. Similarly, BTC and mag-fura-2 [51] (K_d~20 μM [52]) reported higher $[Ca^{2+}]_i$ than fura-2 in neurons exposed to NMDA [49,53-56] or a stimulus train [57,58] .

While alternative explanations are conceivable [59-62], substantial Ca^{2+} buffering by high affinity indicators has been suggested as the main reason [53,56,63]. While indicator-ion binding may be regarded as a "necessary evil" in most calcium imaging experiments, several studies have shown how indicator related distortions could be used to gain insights into the nature of endogenous buffers and free calcium traces [38,64-66]. For various reasons, however, application of these methods to the majority of routine calcium imaging experiments has not been a practical proposition. Consequently, results of these studies may be affected by the presence of an indicator. To address this problem, we have developed and tested a simple, steady-state model-based method to account for indicator effects on the amplitude of calcium signals.

Material and Methods

In Vitro Experiments

In vitro experiments were performed in solutions containing 100 mM KCl, 10 mM MOPS, 1 mM Mg^{2+} in which desired concentrations of Ca^{2+} were obtained by cross-diluting 10 mM EGTA and 10 mM CaEGTA standard solutions (Invitrogen Carlsbad, CA) or self-prepared and tested as described previously [67], using a protocol provided by Invitrogen. The concentration of free Ca^{2+} ions was independently verified using a calcium-selective electrode (Model 97–20, Orion Research Inc., Beverly, MA). After adding fura-2, the measurement was repeated with the ion selective electrode and fura-2 microfluorometry in 20 μm thick glass capillaries (VitroCom, Mountain Lakes, NJ) using an imaging system described below.

Cultures Of Primary Hippocampal Neurons

Cell cultures were prepared as described previously [68]. Briefly, hippocampi removed from 0–3 postnatal day Sprague Dawley rat pups were treated with papain (1 mg/ml) and mechanically triturated. Cells were then plated in type I collagen coated (0.5 mg/ml) 35 mm glass-bottom dishes (Cell E&G, San Diego, CA) ~650 cells/mm2 and cultured in Eagle's medium supplemented with serum, D-glucose, glutamine, and antibiotics at 37°C in a humidified incubator. Cytosine arabinoside (6.7 μM) was added 3–4 days after plating to inhibit cell division. Cells were imaged 14–16 days after plating.

Imaging Experiments

All imaging experiments were carried out at room temperature in a HEPES-buffered salt solution (HCSS) containing, in mM: 141 NaCl, 5.4 KCl, 1 NaH_2PO_4, 1.8 $CaCI_2$, 1 $MgSO_4$, 12 HEPES, and 5.5 D- glucose, pH of which was adjusted to 7.35±0.05 with 0.1 M NaOH. Cells were loaded with fura-2 (Teflabs, Austin, TX) at room temperature by incubation with 10 μM AM ester in the presence of 0.1% Pluronic F-127 (Invitrogen), washed and incubated for another 30–60 min to allow for ester processing. After loading, cells were imaged on an inverted microscope (Nikon Eclipse TE300; Nikon, Melville, NY) equipped with a cooled CCD camera (Cooke, Auburn Hill, MI) using a 20x/0.75 S Fluor objective (Nikon). The fluorescence excitation (75 W xenon arc lamp) was delivered via band-specific filters (340 and 380 nm; Semrock, Rochester, NY) in combination with a XF73 dichroic beam splitter (Omega Optical, Brattleboro, VA). Pairs of images were collected at 5 sec intervals at alternate excitation wavelengths. After subtracting the matching background, image intensities were divided by one another to yield ratio values (R) for individual cells. $[Ca^{2+}]_i$ in individual cells was calculated using formula [14]:

$$\left[Ca^{2+}\right]_i = K_d \times B \times \left(R - R_{\min}\right) / \left(R_{\max} - R\right) \quad (1)$$

where K_d is the indicator dissociation constant for Ca^{2+} (0.22 μM) [14]; R is the ratio of fluorescence intensity excited at 340 and 380 nm; Rmax and Rmin are the ratios of Ca^{2+} -bound and Ca^{2+} -free fura-2, respectively, and B is the ratio of the fluorescence intensity of the second excitation wavelength at zero and saturating Ca^{2+} concentrations [14]. The calibration constants (R_{min}, R_{max}, and B) were determined at the end of each experiment by exposing the cells first to 10 μM 4-Br-A23187 (Teflabs) and then to 10 mM EGTA. Cells that failed to respond to stimulation or provide calibration data were excluded from further calculations.The desired intracellular fura-2 concentrations were achieved by varying the time of indicator loading (15-180 min) and assessed by comparing cell fluorescence intensity excited at 360 nm to that of a 20 μm thick microslide filled with 0.1 μM free Ca^{2+} calibration buffer [67]. Image acquisition was controlled by Metafluor (Molecular Devices (San Jose, CA) and data processing was performed using a scientific graphing program SigmaPlot (Systat, Chicago, IL).

Modelling and Data Processing.

All simulations and numeric solutions to equations mentioned in text were created using Mathematica (Wolfram Research, Urbana-Champagne, IL). The calculated parameters were generated using Monte Carlo methods [69] Briefly, after adding first a random scatter to the data, the procedure was repeated 1000 times to determine the parameters. We determined median and median deviation for each parameter after rejecting values outside 2.5 and 97.5 percentile. The graphing software (SigmaPlot, Systat, Chicago, IL) was used for all basic data analysis and graph preparation.

Indicators and chemicals

Acetoxymethyl (AM) esters and K^+ salts of fura-2 and 4-Br-A23187 were kind gifts from Dr. A. Minta (Teflabs, Austin, TX, USA). Ca^{2+} calibration kits were bought from Invitrogen. All other chemicals, including EGTA and MOPS, were purchased from Sigma (St. Louis, MO, USA).

Results

Effect of an Indicator on Free Ion Concentration

Fluorescent indicators are used to measure cytosolic concentrations of free metal ions whose native concentrations can vary over a wide range, from ≤10-9 M (e.g.Zn^{2+}) to ≅10^{-1} M (e.g. N^{a+} and K^+). Regardless of these differences, the measurements are typically performed with indicator concentrations (dye) ranging from 30-150 μM, which are needed to provide sufficient signal for accurate intensity measurements. An indicator in such concentrations, however, may bind a substantial fraction of available ions creating a significant difference between the ion concentration before (ion_o) and after (ion_{free}) adding an indicator (Figures 1-3 and supplementary Figure 1A). As determining the former is the ultimate goal of many experiments, and routine measurements provide only the latter [14], it is critically important to find out if and when the difference between iono and ionfree may become large enough to affect the interpretation of experimental results.

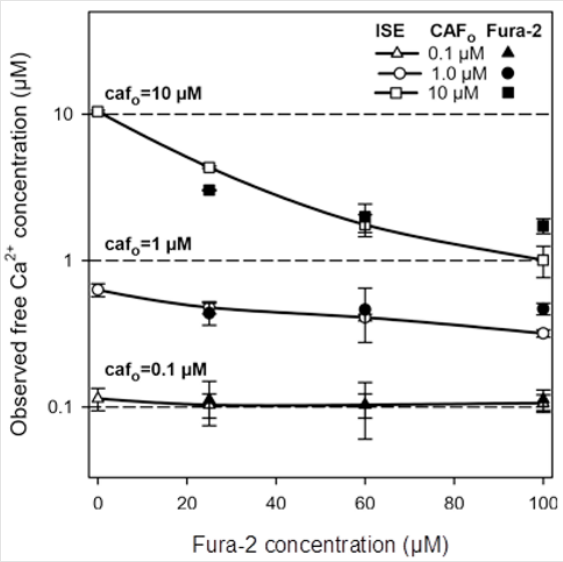

Figure 1: The reduction of free calcium concentration by fura-2 in EGTA-buffered solutions.
The free calcium concentrations in EGTA (500 μM) buffered solutions in the presence of fura-2 were determined with calcium selective electrode (ISE; open symbols) and standard fura-2 microfluorometry [14] (filled symbols). The measurements were repeated 3-4 times in solutions featuring native free Ca^{2+} concentrations (caf_o; horizontal dashed lines) of 0.1 μM (triangles), 1 μM (circles) and 10 μM (squares) and presented as mean (±SD) values. The results for cafo of 0.33μM and 0.33 are not shown.

 DOI: 10.26717/BJSTR.2023.53.008398

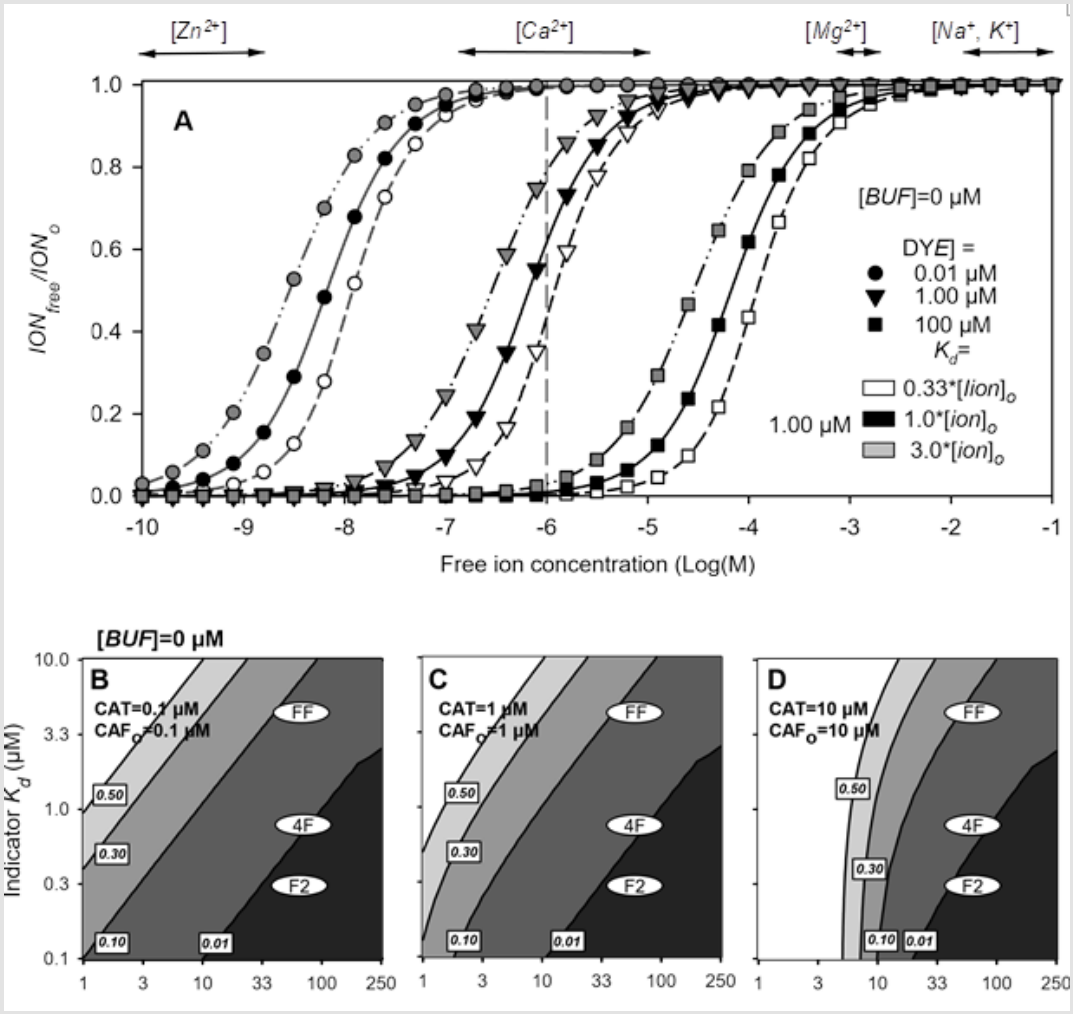

Figure 2: The effects of "smart" (A) and fixed affinity (B-D) fluorescent indicators on the free metal ion concentration in the absence of intrinsic buffering.

- A: The fractions of metal ion concentration that would remain free in the presence of 0.01 µM (circles), 1 µM (triangles) and 100 µM (squares) "smart" indicator featuring low (K_d=3.0*ion$_o$, gray symbols), moderate (K_d=1.0*ion$_o$), black symbols) or high (K_d=0.33*ion$_o$, white symbols) affinity for the measured ion. The presented data were created by solving Eqn.3. Vertical dashed line marks iono =1.0 µM considered in section 3.1. The approximate concentration ranges of biologically relevant metal ions commonly measured with fluorescence indicators are shown for comparative purposes.
- B-D: The effect of fluorescent indicator affinity and concentration on the fraction of Ca^{2+} ions that would remain free (caf_{free}/caf_o) in unbuffered solutions containing 01 µM (B), 1 µM (C) and 10 µM (D) calcium. The selected ratios were marked as solid lines with the caf_{free}/caf_o values shown in white boxes. The caf_{free}/caf_o that would be reported in such systems by commonly used indicator fura-2 (F2; K_d=0.22 µM [14]) and its lower affinity derivatives fura-4F (4F; K_d=0.88 µM [9]) and fura-2FF (FF; K_d=6.0 µM [52]) in concentrations used in imaging experiments are shown as white ovals.

DOI: 10.26717/BJSTR.2023.53.008398

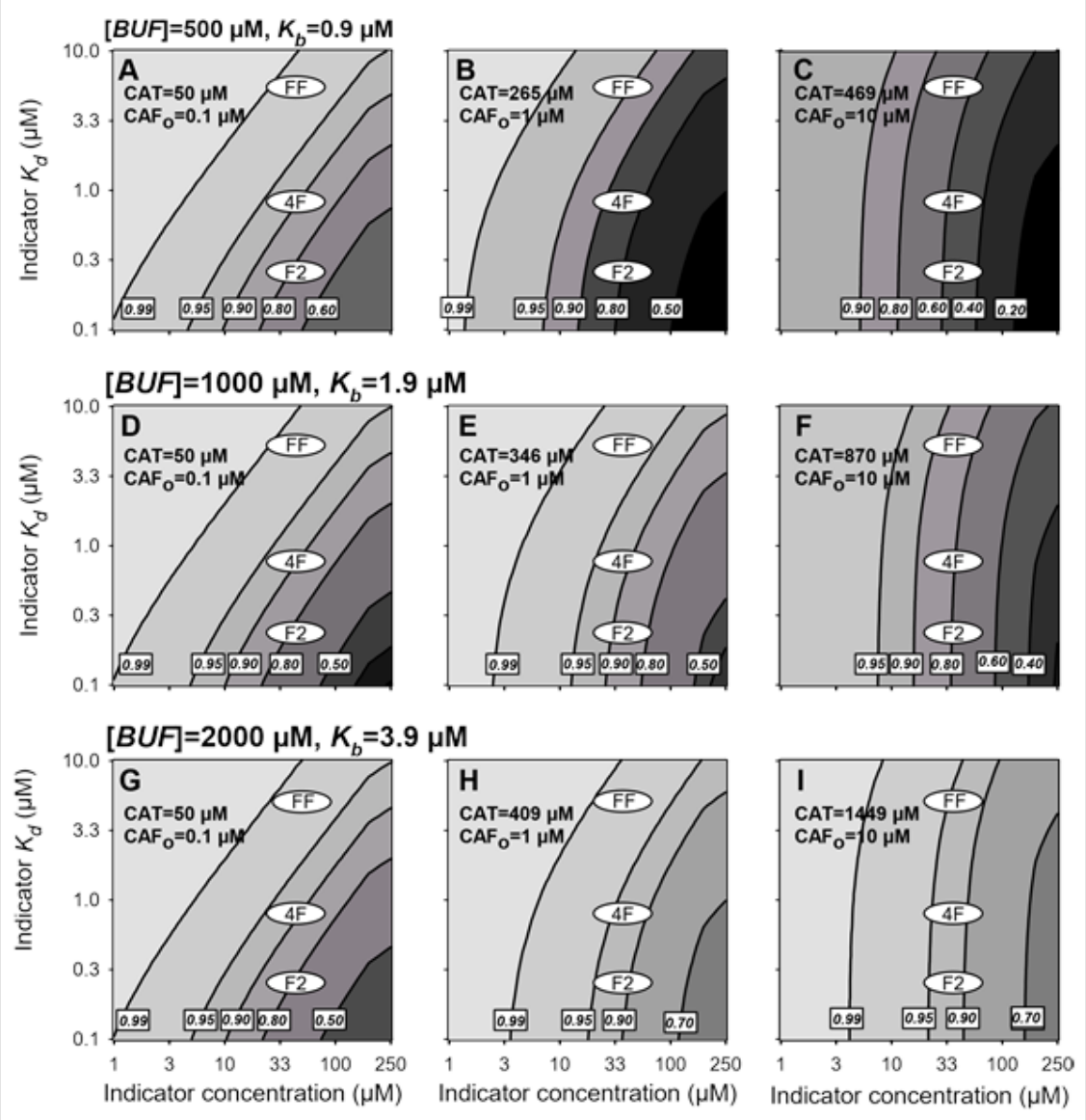

Figure 3: The impact of fluorescent indicators on the free calcium concentration in the presence of endogenous buffers.
The contour plots show the fractions of the true free Ca^{2+} concentrations (caf_o) that would remain free (caf_{free}) after adding fluorescent indicators to calibration solutions in which cafo of 0.1 µM (A, D, G), 1.0 µM (B, E, H) and 10.0 µM (C, F, I) is maintained with low (G-I), medium (D-F) or high (A-C) affinity endogenous buffers. The simulations were created by numerically solving Eqn. 10b for sets of indicated conditions (please see sections 3.1 and 3.2 for details). Annotated solid lines show selected caf_{free}/caf_o ratios and the white ovals encompass values likely to be reported by fura-2 (F2; K_d=0.22 µM), fura-4F (4F; K_d=0.88 µM) and fura-2FF (FF; K_d=6.0 µM) in typical concentrations (30-100 µM) used in imaging experiments.

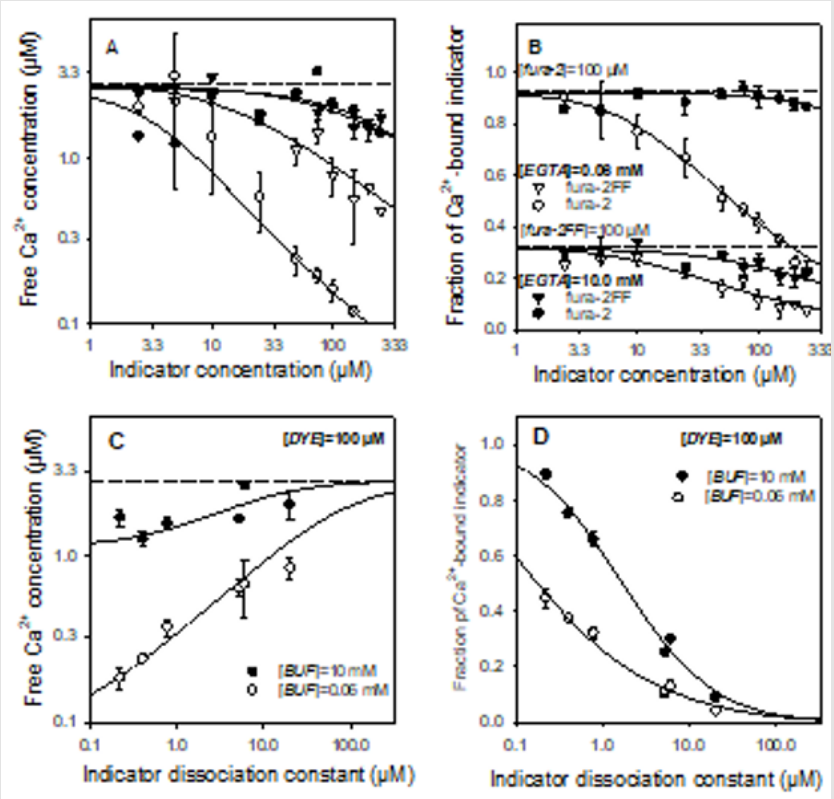

Supplementary Figure 1: Calcium indicators reduce free Ca^{2+} concentrations as dictated by their concentration and affinity.

- A-B: Using standard imaging techniques, we determined free Ca^{2+} concentrations (caf_{free}) (A) and fractions of Ca^{2+}-bound indicators (?) (B) of fura-2 (K_d=0.22 μM, circles) and fura-2FF (K_d=6 μM, triangles) in solutions containing either 10 mM (filled symbols) or 60 μM (open symbols) EGTA, but the same free Ca^{2+} concentration (caf_o =2.85 μM) as determined with an ion selective electrode.
- C-D: In analogous experiments, we determined caf_{free} (C) and (D) of several fura-2 like indicators (dye=100 μM) featuring different affinities for calcium (0.22 μM ≤K_D≤20 μM),) in a well (filled circles) and poorly (open circles) buffered solutions. The presented data (mean ± SE) were pooled from 3-5 independent experiments.

To examine this issue, let us first consider a situation in which only an indicator can bind measured ions. A situation that assumes a simple 1:1 stoichiometry can be described by the following reaction:

$$ION + DYE \rightleftarrows ION * DYE \quad (2)$$

At equilibrium, the concentration of free ions (ion_{free}) can be expressed as [31]

$$ion_{free} = \frac{1}{2} * \left(ion - dye - k_d + \sqrt{(ion_o - dye - K_d)^2 + 4 * ion_o * K_d} \right) \quad (3)$$

where ion and dye are the total ion and indicator concentrations, respectively, and K_d is the indicator apparent dissociation constant [31]. To make this equation applicable to a wide range of conditions and avoid indicator saturation, we first consider a hypothetical "smart" sensor whose K_d corresponds to the total and, in the absence of any buffering agents, also to the native ion concentration (ion_o).

Such an indicator (30 -150 μM) will not significantly reduce the free concentrations of ions whose intracellular levels fall in the milimolar range (i.e.Na+, K^+ and possibly Mg^{2+}), irrespective of its affinity for the measured ions (Figure 2A). In contrast, much lower indicator concentrations (dye<1 μM) would be sufficient to bind a vast majority of free Zn^{2+} and, to a lesser extent, Ca^{2+} ions (Figure 2A). Here, especially in the case of calcium whose native concentrations (caf_o) range from ~0.1 μM in resting to 10 μM or even 100 μM in stimulated cells, the accuracy of the measurement (ion_{free}/ion_o) depends not only onion and indicator concentrations, but also on the dye dissociation constants. At this ion concentration range, low affinity probes yield markedly higher ion_{free} values than their high affinity counterparts (Figure 2A). For example, a standard "smart" indicator would report the caf_o of 1 μM as either 0.99 μM or 0.01 μM when present in low (0.01 μM) or high (100 μM) concentrations (Figure 2A, black circles and squares), respectively. Likewise, the same caf_o of 1 μM would be reported as 0.42 μM or 0.79 μM by the high (K_d=0.33 μM) or low (K_d=3 μM) affinity indicator (dye=1 μM; Figure 2A; vertical dashed line, white and gray triangles). Taken together these data illustrate how an indicator that can freely bind the ions it is supposed to measure can significantly reduce their free concentrations and report values (ion_{free}) markedly lower than those in the absence of the indicator

whenever its concentration exceeds 10-20% of iono. Lowering probe affinity alleviates, but does not completely avoid the indicator buffering effect.

To put these data in perspective, we repeated the simulations for real-life, fixed affinity fluorescent indicators for 0.1 μM, 1 μM and 10 μM free Ca^{2+}, concentrations corresponding to cytosolic free calcium levels in resting and stimulated cells. Indicator concentrations (1 μM <dye<250 μM) and dissociation constants (0.1 μM <K_d<10 μM) were selected to encompass those encountered in typical calcium imaging experiments and include commonly used indicators - fura-2 (K_d=0.22 μM) and its low affinity analogues, fura-4F (K_d=0.8 μM) and fura-2FF (K_d=6 μM) (Figures 2B-2D and Supplementary Figure 1B). It is worth noting that fura-2 and its low affinity analogue, fura-2FF at typical concentration of 50-100 μM would report caf_{free} corresponding to merely 1% and 10-20% of caf_o, respectively, for all considered caf_o values (Figures 2B-2D).

The Role of Endogenous Buffers

In the absence of an indicator, the steady-state intracellular free Ca^{2+} concentration (caf_o) is maintained by a balance between all available calcium ions (cat) and a variety of calcium binding proteins (CBP) [24,70]. Once introduced to a cell, an indicator, itself a calcium buffer competes with the endogenous buffers for the same pool of ions, which creates a new equilibrium and sets up a new free calcium level (caf_{free}). This process can be described by a reaction

$$Ca_o^{2+} + BUF_{free} + DYE_{free} \rightleftarrows Ca_{free}^{2+} + BUF_{ca} + DYE_{ca} \quad (4)$$

In which BUF and DYE refers to endogenous buffer and an indicator, respectively. The total pool of Ca^{2+} ions is split between the buffer (BUF_{Ca}) and the indicator (DYE_{ca}) with some ions remaining free (Ca_{free}^{2+}). Assuming a simple 1:1 stoichiometry, total concentrations of calcium ions (cat), buffer (buf) and indicator (dye) can be expressed as sums of their free (caf_{free}, buf_{free}, dye_{free}) and calcium bound (buf_{ca}, dye_{ca}) forms

$$cat = caf_{free} + buf_{ca} + dye_{ca} \quad (5a)$$

$$buf = buf_{fee} + buf_{ca} \quad (5b)$$

$$dye = dye_{free} + dye_{ca} \quad (5c)$$

At equilibrium, the relationship between concentrations of free calcium ions (caf_{free}), free buffer (buf_{free}) and the Ca* BUF complex (buf_{Ca}) is determined by the dissociation constant (K_b) and defined as:

$$K_b = \frac{caf_{free} * buf_{free}}{buf_{Ca}} \quad (6)$$

Consequently, the concentration of Ca*BUF complex can be expressed as

$$buf_{ca} = \frac{caf_{free} * buf_{free}}{K_b} = \frac{caf_{free} * (buf - buf_{ca})}{K_b} \quad (7)$$

which is equivalent to

$$buf_{ca} = \frac{caf_{free} * buf}{caf_{free} + K_b} \quad (8)$$

and by analogy the concentration of Ca^{2+}-bound indicator (dye_{Ca}) can be expressed as

$$dye_{ca} = \frac{ccaf_{free} * dye}{caf_{free} + k_d} \quad (9)$$

where K_d is the dissociation constant of the DYE_{Ca} complex.

Substituting equations 8 and 9 into equation 5a yields expressions

$$cat = caf_o * \left(1 + \frac{buf}{caf_o + K_b}\right) \quad (10a)$$

$$cat = caf_{free} * \left(1 + \frac{buf}{caf_{free} + K_b} + \frac{dye}{caf_{free} + K_d}\right) \quad (10b)$$

that define the relations between the total (cat) and free (caf) calcium concentrations in the presence of endogenous (buf; Eqn.10a) and of both endo- and exogenous (dye; Eqn.10b) buffers with known affinities for calcium (K_b and K_d).

To examine these relationships more closely, we numerically solved Eqn. 10b for a set of conditions (section 3.1; Figures 2B-2D) assuming that caf_o was maintained by low, medium or high affinity intrinsic buffers (Figure 3). The buffer concentrations were chosen to provide the same buffering capacity of 500 for caf_o=0.1 μM; (Figure 3A, D, G). The same buffer concentrations were subsequently used for caf_o of 1 μM (Figures 3B, 3E, 3H) and 10 μM (Figure 3C, F, I). The simulation results show that all considered indicators might be expected to yield caf_{free} higher than 90% of caf_o as long as the calcium concentration remains low (Figures 3A-3C). This is no longer the case when caf_o exceeds the buffering range of the intrinsic buffer (caf_o>>3*K_b) and Ca^{2+} ions can be more or less freely sequestered by an indicator. Here, just as in the absence of endogenous buffers (Figures 2B-2D), low affinity indicators, which bind fewer ions, report markedly higher caf_{free} than high affinity ones, especially in the presence of high affinity buffer (Figure 3, Supplementary Figure 1C).

In summary, low caf_o can be estimated quite accurately with almost any indicator, regardless of the properties of the endogenous buffers (Figures 1, 3A, 3D, 3G). However, as cafo rises, caf_{free} becomes increasingly dependent on the complex relations between intrinsic and exogenous buffers (Eqn. 10b) and thus more likely to deviate markedly from caf_o (Figures 1 & 3). The magnitude of this difference cannot be easily assessed without having, at least, rudimentary knowledge of the properties of the endogenous buffers. As a standard approach (Eq. 1) [14] does not consider this, the calculated caf_{free} represents only a caf_o estimate of uncertain accuracy.

Determination of the Native Ca^{2+} Concertation and Intrinsic Buffer Properties

Among the terms (dye, K_d, caf_{free}, buf, caf_o, and K_b) in Eqn.10b, only the first three are, at least in principle, known or controlled by the observer. The indicator concentration depends on the loading conditions and can be estimated by measuring fluorescence intensity [67]. The indicator dissociation constant (K_d) is determined by the choice of indicator, which is typically already well characterized [10,11] or can be measured in separate *in vitro* or in situ experiments. Finally, the free Ca^{2+} concentration (caf_{free}) is derived from the indicator signal using the standard approach [14]. The other parameters, which include Ca^{2+} concentrations, cat and caf_o, along with the concentration and affinity of the intrinsic buffer, are unknown and have to be determined.

Non-Linear Regression Analysis: As higher indicator concentrations tend to report lower caf_{free} values (Figure1, Supplementary Figure 1), we hypothesized that the true indicator independent free calcium concentrations (caf_o) and other system parameters (cat, buf, K_b) may be accurately estimated by extrapolating caf_{free} values to the indicator-free environment. To test this hypothesis, we analyzed the data (Figure 1) using the "least square method" to minimize the function

$$\sum_{k=1}^{n}\sum_{i=1}^{m}\left(caf_{k,i}*\left(1+\frac{buf}{K_b+caf_{k,i}}\right)-caf_{k,i}*\left(1+\frac{buf}{K_b+caf_{k,i}}+\frac{dye_i}{K_d+caf_{k,i}}\right)\right)^2=0 \quad (11)$$

for k and i distinct calcium (cat) and indicator (dye) concentration s, respectively.

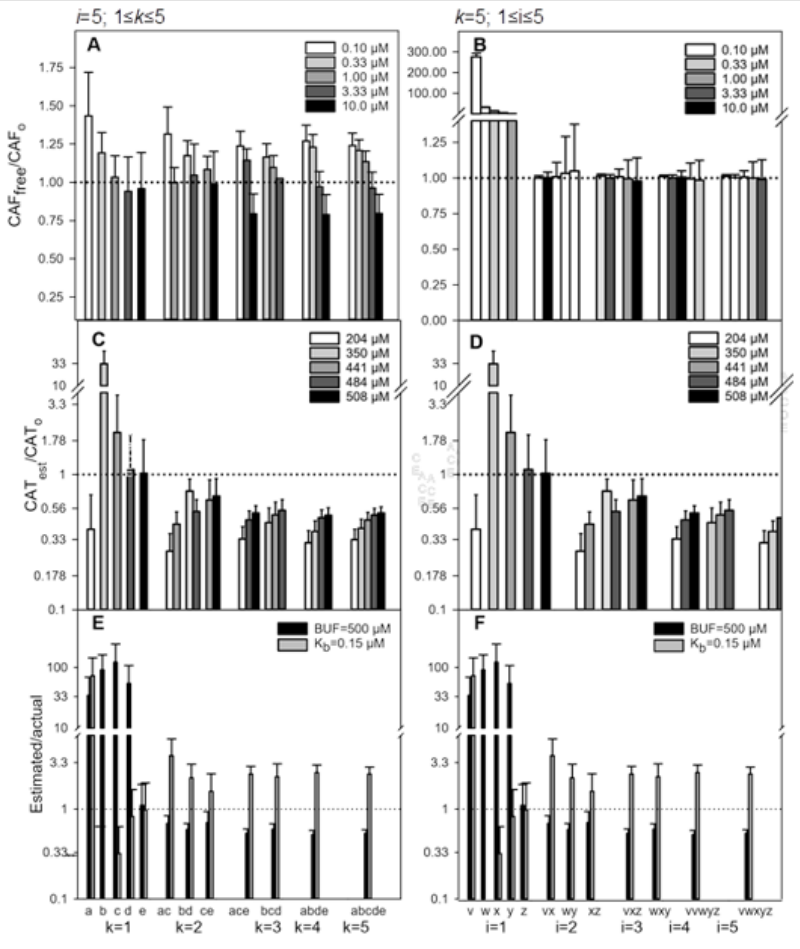

Figure 4: Characterization of the EGTA-buffered model systems with a multiple nonlinear regression - the role of the number of tested calcium (k) and indicator (i) concentrations.

- A-B: The true free Ca^{2+} concentrations determined by solving Eqn. 11 for sets of data collected in k EGTA buffered solutions (0.1 µM <caf_o≤10 µM) using five fura-2 concentrations (i=5, dye=25-100 µM) (A) or gathered with i fura-2 concentrations (25 µM<dye<100 µM) in five calibration solutions (k=5; 0.1 µM <caf_o≤10 µM) (B).
- C-D: The estimated total Ca^{2+} concentrations (cat) calculated as described above.
- E-F: Concentrations and dissociation constants of the endogenous buffer estimated as described above.

After running 1000 iterations and rejecting the extreme results outside 2.5% -97.5 percentile, the data have been pooled together, divided by the actual values, and shown as the ratio (median ± median deviation). Horizontal dotted lines represent a situation when the calculated values are equal to the actual ones. The letters (cafo in µM: a-0.1, b-0.33, c-1, d-3.3, e-10; dye in µM: v-25, w-37.5, x-50, y-75, z-100) underneath the bars show which single datasets (k=1, or i=1) or their combinations (2≤k≤5, e.g. ace; 2≤i≤5; e.g. vxzj) have been used to create presented data. Please note the difference in y-axis scales.

The effectiveness of this procedure may depend on the number of available datasets defined as either a number of different cat (k) probed with a single indicator concentration (i=1) or a number of distinct dye concentrations (i) used to measure a unique caf_o level (k=1) (Figure 4). In addition, regression results are bound to be affected by data (caf_{free} and dye) scatter (Figure 5). As the model systems contain several different calcium concentrations maintained by the same buffer (EGTA; dye=500 µM, K_b=0.15 µM), the procedure returns as many caf_o and cat estimates as considered datasets (k), but only single buf and K_b value for each analyzed dataset array regardless of the number of indicator concentrations (i) (Figures 4A, 4C, 4E). Similarly, calculations utilizing data collected with i indicator concentrations in five solutions with different caf_o (k=5) return five caf_o and cat, but only single buf and K_b estimates (Figures 4B, 4D, 4F).

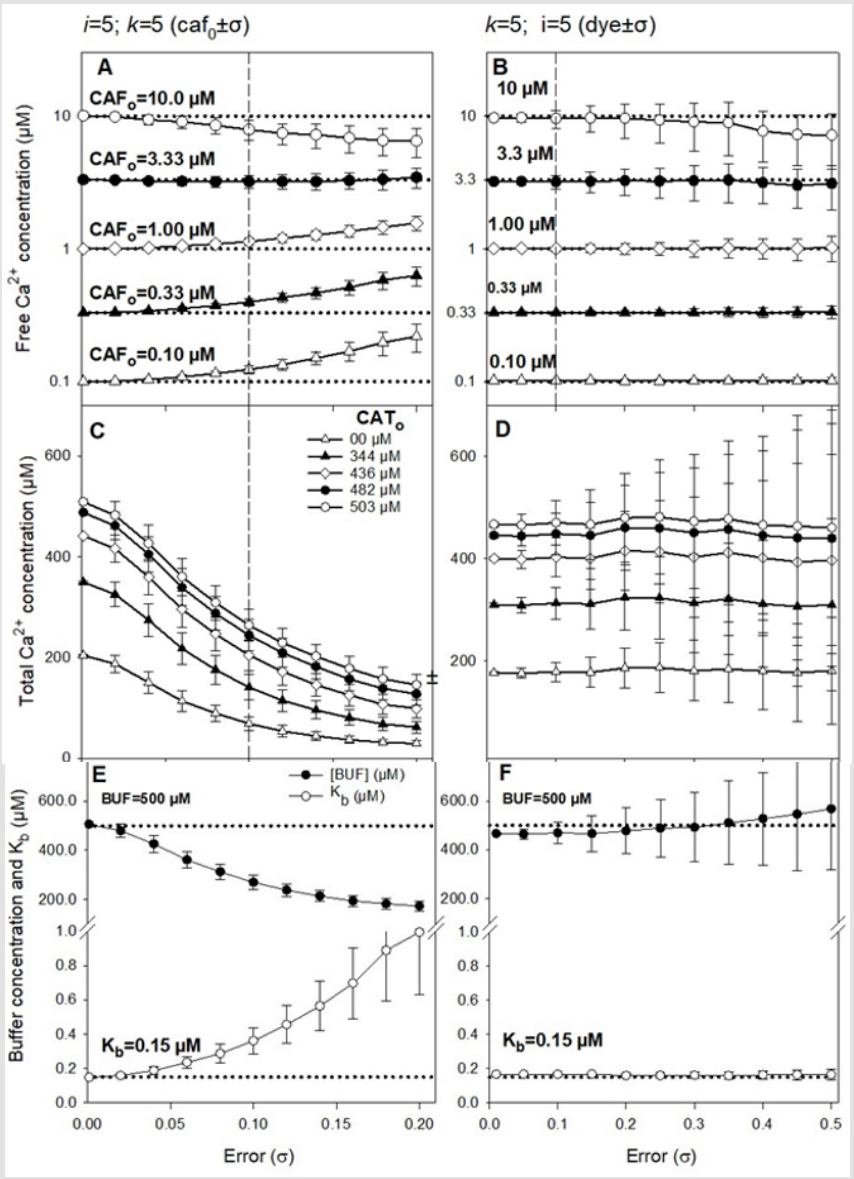

Figure 5: The impact of data scatter on the accuracy of the multiple regression method.

- A-B: The true free Ca^{2+} concentrations (caf_o) were determined by solving Eqn.11 using all available data (i=k=5) modified by adding a normally distributed variate with standard deviation (σ) either to the caf_{free} (A) or dye (B).for simplicity, the other parameter (e.g. dye in A) remained unmodified. After running 1000 iterations and rejecting the extreme results outside 2.5%-97.5 percentile, the data have been averaged and presented as median± median deviation. Horizontal dotted lines correspond to the actual cafo values.
- C-D: The total calcium concentrations (cat) were calculated as described and presented (median± median deviation) as a function of caf_{free} (C) and dye (D) variability (σ).
- E-F. Estimates of the concentration (buf; filled circles) and dissociation constant (K_b; open circles) of the endogenous buffer (median± median deviation) derived from increasingly scattered (σ) caf_{free} (E) and dye (D) data.

If the data collected with all five indicator concentrations (i=5) are taken into account, the regression procedure estimates caf_o quite well regardless of the number of considered Ca^{2+} or their arbitrarily chosen combinations (Figure 4A). Using caf_{free} data from two or more solutions featuring different calcium content (k≥2) reduces the scatter of the estimated caf_o values, but does not avoid overestimating low, and underestimating high, caf_o values (Figure 4A). On the other hand, caf_{free} determined with at least two distinct indicator concentrations (i≥2) are required for accurate caf_o estimates in a system comprising five different Ca^{2+} concentrations (Figure 4B). Likewise, to estimate the total calcium concentration and properties of endogenous buffer, the regression analysis must include caf_{free} measured with at least two indicator concentrations in five test solutions (i≥2, k=5) or, alternatively, two solutions with five indicator concentrations (k≥2, i=5). If these minimal requirements are met or exceeded, regression analysis underestimates cat (Figures 4C, 4D) and buf (Figures 4E, 4F; black bars), but overestimates K_b (Figure E, F; grey bars)

To assess the impact of data scatter, on regression results, we analyzed all experimental data (k=i=5) after gradually raising their variability (Figure 5). Analysis of the nearly perfect data (Figure 5 σ =0) provides good estimates of all parameters, but as the data, particularly caf_{free}, scatter increases, the accuracy of parameter determination begins to decline. The estimated caf_o, the most stable parameter, becomes progressively higher (Figure 5A, open triangles) or lower (Figure 5A, open circles) than actual values. The total Ca^{2+} concentrations (Figure 5C) tend to be underestimated with higher values being relatively less affected. Finally, increasing the caf_{free} variability leads to describing the endogenous buffer as weaker and less abundant than it actually is. (Figure 5E) and in consequence leads to underestimating its buffering capacity (data not shown). In contrast, increasing the variability (i.e. decreasing the accuracy) of indicator concentration determination, seems less consequential. Here, the estimated parameters are little affected by growing data scatter, but the confidence intervals, particularly those of buf and cat, become broader (Figures 5B, 5D, 5F).

In summary, non-linear regression can provide estimates of the Ca^{2+} concentrations and intrinsic buffer characteristics in an experimental system if at least two datasets (k≥2 or i≥2) are used for analysis. In this case, regression estimates of the true free Ca^{2+} concentration and approximates, albeit with a lesser accuracy, cat, buf and K_b. The accuracy of the estimates depends on the precision of caf_{free} rather than dye determination. Consequently, contingent on the magnitude of experimental errors, regression results may constitute accurate estimates or just represent the lower or upper limits of the actual values.

Linear Approximation: To avoid complexities involved in solving equation 11, which requires specialized software, we have converted equation 10b into a linear form

$$cat = caf + caf * bc + \propto * dye \quad (12)$$

in which bc= $buf/(K_b+caf_{free})$ and α= $caf_{free}/(K_d+ caf_{free})$ denote the buffering capacity of the intrinsic buffer and the fraction of Ca^{2+}-bound indicator, respectively. Solving this equation for dye yields a simple linear function (y=a*x+b) in which y=dye, x=1/α, a=cat and b=- caf_{free} / α - caf_{free} *bc/ α =- caf_{free} / α *(1+bc) =-(K_d+ caf_{free})*(1+bc). Assuming that the indicator concentrations (dye) and corresponding fractions of Ca^{2+}–bound indicator (α) have been experimentally determined (Figure 1), analyzing this relationship (Eqn.12) provides estimates of the cat and caf_o. While the former is determined directly as a slope (a=cat), the latter can be calculated from the x-intercept of the regression line (dye=0, caf_o=K_d* α_0 /(α0-1)) (Figure 6A). Once the caf_o, cat and K_d are known, the buffering capacity (bc) can be calculated from the y-intercept b (bc=-b/(caf_o+K_d)-1) or, alternatively, as the ratio of total and free calcium concentrations (bc=cat/caf_o-1). The procedure provides accurate estimates of caf_o (Figure 6B, grey bars) and underestimates cat and bco (Figure 6A, white and black bars) as long as the measured Ca^{2+} concentrations remain lower than 10 μM, at which point the calculated parameters, particularly caf_o and bc, deviate markedly from the actual values (Figure 6B). This loss of accuracy may arise from assuming that the free term b in equation12 is independent on caf_{free}, a simplification necessary for problem linearization. Once this procedure is repeated in several systems with the same intrinsic buffer but different Ca^{2+} concentrations, the relationship between the formerly determined values of bc and caf_o can be analyzed to estimate the concentration and affinity of the endogenous buffer. This time, the definition of the buffering capacity (bc=$buf/(K_b+caf_o)$) is converted into a linear form

$$caf_o = buf * \frac{1}{bc_o} - K_b \quad (13)$$

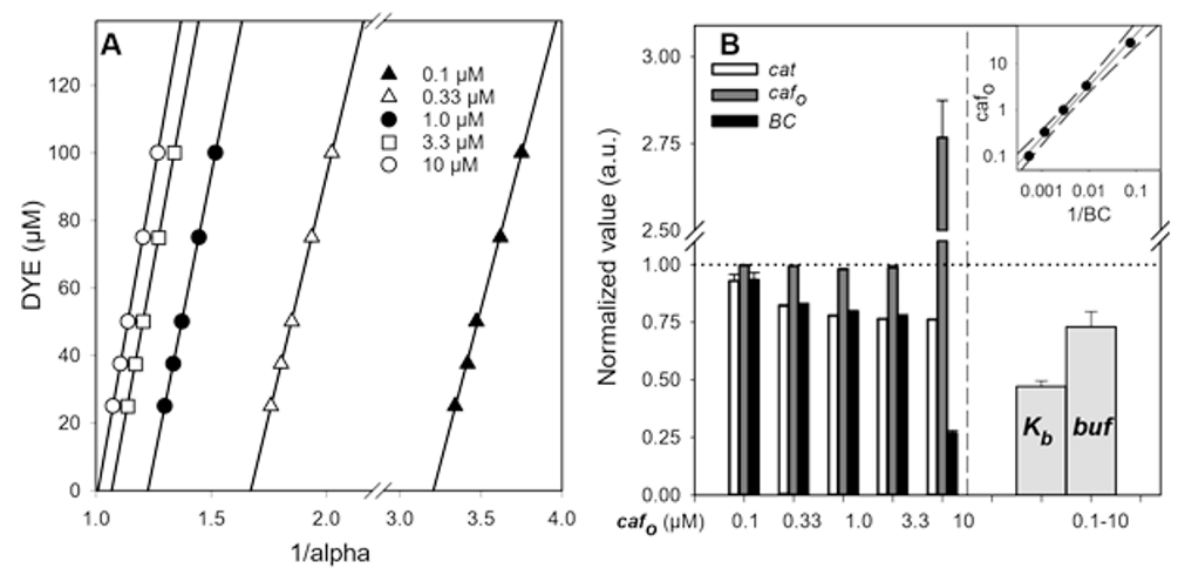

Figure 6: Linear regression approach to determine the calcium concentrations (cafo) and intrinsic buffer properties in a model system.

- A: Linear relationships between the free Ca^{2+} concentrations (caf_{free}) determined in model stems (Figure 1) and converted into the reciprocals of the Ca^{2+}-bound indicator fractions (1/alpha) as described in section 3.3.2 and fura-2 concentration (dye). The presented data (mean±SD) were pooled from 3-4 experiments.
- B: Total (cat; white bars) and true free Ca^{2+} concentration (caf_o; dark grey bars) and the buffering capacity (BC; black bars) derived from the linear regression analysis of each dataset shown in panel A (see section 3.3.2). The concentration (buf) and the dissociation constant (K_b) of endogenous buffer (light grey bars) were determined by regression analysis (inset) of the formerly determined caf_o and BC values (A). The error bars represent 95% confidence intervals for the regression-derived parameters (B). To facilitate comparisons, all estimated parameters were divided by the actual values and presented as normalized data. The situation when the estimated values are equal to the actual ones is presented by a horizontal dotted line. The auxiliary vertical dashed line separates the results yielded by the primary (A) and secondary (B inset) linear regression procedures.

In which the dependent ($y=caf_o$) and independent ($x=1/bc_o$) variables are known. The slope and the y intercept determined by the regression analysis correspond to the buffer concentration (buf) and the buffer dissociation constant (K_b), respectively (Figure 6B inset). As the analyzed data, caf_o and bc_o, are just estimates derived from another regression procedure (Eqn. 12), the results, buf and K_b differ somewhat from the actual values (Figure 6B, light grey bars).

Cellular Data

To test this approach in situ, we measured free Ca^{2+} concentrations $[Ca^{2+}]_i$ with fira-2 in cultured neurons subjected to brief depolarization with 50 mM K^+ using a standard method (Eqn.1). These values (caf_{free}) proved to be heavily dependent on fura-2 concentration (Figure 7A): the higher it was, the lower were the peak caf_{free} values and their dissipation rates (Figure 7A, filled circles). While fura-2 concentration effect was evident in cells featuring elevated Ca^{2+} levels (Figure 7A), the indicator also reduced free Ca^{2+} levels in resting neurons (Figure 7C, black bars), patterns predicted by the theoretical models (Figures 2 & 3) and observed in *in vitro* buffer systems (Figure 1, Supplementary Figure 1A). Using the methods described in section 3.3.1 and 3.3.2., we analyzed the relationship between selected caf_{free} values (Figure 7A, asterisks) and indicator concentrations. This approach efficiently corrected the peak amplitude, but not the time course of calcium change (Figure 7A, open circles). The estimated caf_o in resting (~22 nM) and stimulated (1.18 μM) neurons (Figures 7A & 7C) are higher than caf_{free} derived from singe measurements (Figure 7C). It seems therefore that routine experiments may provide accurate caf_o estimates only if carried out with much lower fura-2 concentrations than the lowest one tested (33 μM). This critical indicator concentration is hardly a universal limit as it may vary depending on the caf_o (Figures 1 & 3), properties of endogenous buffer (Figure 3) and indicator itself (Supplementary Figure 1C).

As indicator concentration increases, so does the gap between caf_{free} and caf_o in both resting and stimulated neurons (Figure 7C). Interestingly, the caf_o in resting neurons with the highest fura-2 concentration (~ 288 μM) is much higher than overall caf_o calculated by analysis of all available data (Figure 7C, horizontal line). The nature of this difference is somewhat unclear. It may result from inaccuracy of the collected data and processing (Figure 5) or reflect an actual effect an indicator at high enough concentrations may exert on calcium homeostasis.

 DOI: 10.26717/BJSTR.2023.53.008398

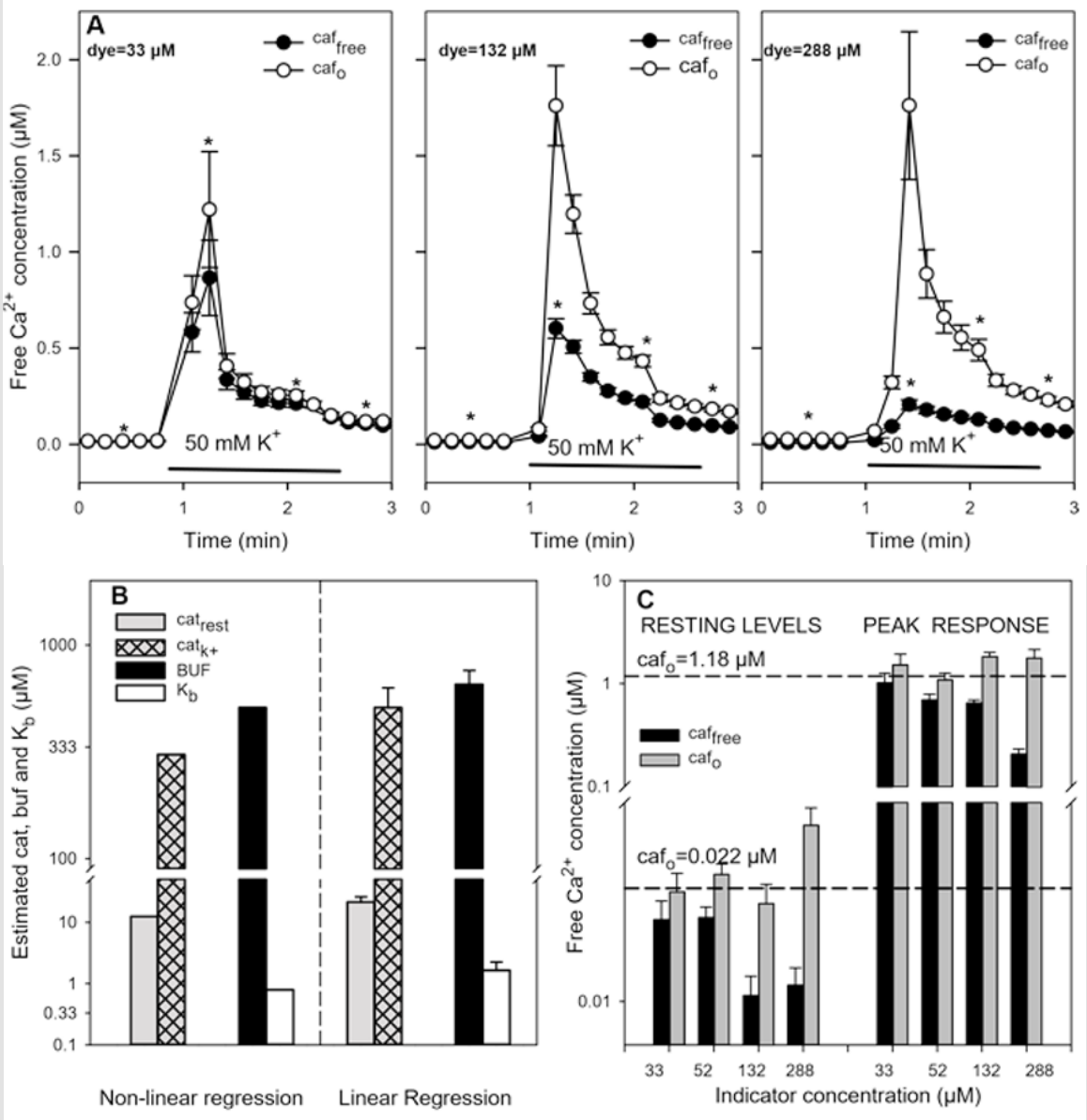

Figure 7: Determination of calcium concentrations and intrinsic buffer properties in rat hippocampal neurons using the multiple regression method.

- A: Free Ca^{2+} concentrations (caf_{free}) were determined in cultured rat hippocampal neurons using standard imaging techniques (Eqn. 1; filled circles) in the presence of indicated fura-2 concentrations (dye) during depolarization with 50 mM K^+. The selected caffree (asterisks, k=4) and dye values (i=4) were then analyzed using non-linear regression (Eqn. 11) to yield the native free Ca^{2+} concentrations (caf_o, A; open circles). The presented data are mean values (± SE) of 34-102 cells pooled from 3-4 experiments. For clarity, only every other point is shown.
- B: The estimates of the endogenous buffer concentration (filled bar), its dissociation constant (open bar) and total calcium concentration in resting (cat_{rest}; light gray bar) and depolarized (cat_{K}^+; light gray hatched bar) neurons were calculated by solving Eqn. 11 for selected caf_{free} and dye data (A, asterisks). For comparison, the same data were analyzed using linear regression. The standard errors of the estimated values are shown only for linear regression, which generates them directly.
- C: The tree Ca^{2+} concentrations in resting and depolarized neurons calculated using the buf, cat and K vales produced by the multiple regression analysis for individual neurons (caf_o; gray bars) are compared to the results of direct measurements (caf_{free}; black bars). The presented data are mean values (± SE) of 34-102 cells pooled from 3-4 experiments The horizontal dashed lines represents the mean true Ca^{2+} concentration (caf_o) generated by the multiple regression analysis of all available datasets (k=4, i=4).

In addition to estimating caf_o, regression analysis provides an estimate of the total Ca^{2+} concentration (Figure 7B, grey bars) and offers an insight into the nature of the generic Ca^{2+} buffer in the cytosol (Figure 7B, black and white bars). We assessed this using both the non-linear regression (Eqn. 11) and its simplified linear version (Eqn. 12 and 13). The multiple regressions estimated the cat in resting and depolarized neurons to be 12.5 μM and 306 μM, respectively. Taken together with the caf_o approximation of 22 nM and 1.18 μM (Figure 7B), we can calculate the buffering capacity as 560-570 in resting cells and ~260 at the peak Ca^{2+} response. Calculating buffering capacity from the concentration of endogenous buffer (buf=509 μM) and its affinity (K_b=0.78 μM) (Figure 7B), provides similar results, 634 and 259, in resting and stimulated neurons, respectively. In turn, the linear regression presented neurons as having somewhat higher concentration (buf=653±150 μM) of a lower affinity buffer (K_b=1.63 ± 0.62 μM) (Figure 7B), which corresponds to buffering capacity of 359 and 232. Although the results generated by both methods are somewhat different (Figure 7B), they are consistent with the consensus that neurons contain relatively high concentrations of a low affinity buffer. In either case, the data indicate that only a very small fraction of Ca^{2+} ions (<0.4%) remains free even when caf_o peaks after depolarization. Even though this buffering system is quite efficient, adding another buffer such as fura-2 can markedly reduce caf_o (Figure 7A).

Although accuracy of data provided by both methods cannot be independently verified, our experiments in model systems (Figure 5) offer some general guidelines for interpretation. In particular, the *in vitro* experiments demonstrate that the caf_o estimates are the least prone to experimental errors (Figures 5A & 5B) with the exception of the non-linear regression being unable to correctly assess the caf_o of 10 μM (Figure 7C). As the depolarization induced Ca^{2+} rise was 8-9 times lower than that, this shortcoming is not likely to affect the results provided by the simplified method. However, such possibility should be taken into account if the considered peak caf_o are high. Regarding other parameters, the accuracy of their determination depends on the data scatter, particularly the variability of caf_{free}. Following the lessons from the *in vitro* experiments (Figure 5), we expect the actual cat and buf to be higher and the K_b to be lower than the calculated values.

Discussion

Fluorescent indicators are convenient tools to determine intracellular concentrations of calcium and other ions. Their application seems to fall into two broadly defined, but distinct categories. The first includes detailed analysis of biophysical aspects of calcium signaling in excitable cells and relies on complex methodology [37,71-76]. The other, by far more popular, strives to examine changes in global calcium concentration in virtually any cell type using standard methods [14] Among many insights gained through the "biophysical" approach, the one regarding "safe" indicator concentrations seems particularly relevant for more generic studies. Namely, it has been postulated that an indicator does not affect and can therefore accurately trace Ca^{2+} signals as long as the calcium binding ratio (κd) [22] remains markedly lower than that of the cytoplasm (κS) [32].

$$k_S = \frac{buf}{K_b} * \frac{1}{\left(1+\frac{caf_o}{K_b}\right)^2} >> \frac{dye}{K_d} * \frac{1}{\left(1+\frac{caf_o}{K_d}\right)^2} = k_d \quad (14)$$

At least in principle, this equation allows determination of the maximum indicator concentration that would guarantee accuracy of the measurements (for recent reviews see [18,32]). However, practical use in experiments has proven difficult for several reasons. First, the equation itself is quite restrictive and calls for using indicator concentrations that are too low to allow accurate fluorescence measurements, and most routine measurements utilizes indicators at much higher concentrations (30-150 μM) [18,32]. Second, not only do κS values vary considerably between different cells and remain unknown in most cases, but they change with Ca^{2+} concentration (Eqn.14). Finally, even if κ_d and κ_S were known, a rather unlikely scenario, it is not clear how to interpret the "κS>>κd" requirement. While a κ_S/κ_d ratio exceeding 1000, a situation common in calibration solutions, certainly meets this condition, it is unclear what the critical value is in cells. In consequence, indicator signals, ratios or normalized intensities, taken directly or converted into $[Ca^{2+}]_i$ 1[14] may be affected by the indicator itself. While the extent of this effect is hard to judge in any particular case, our data demonstrate the complexity of the effect and suggest that large $[Ca^{2+}]_i$ rises in the presence of high affinity buffer are most likely to be influenced by high affinity indicators (Figure 3, Supplementary Figure 1).

These observations are relevant for two most common categories of routine calcium imaging experiments. When used to compare $[Ca^{2+}]_i$ changes induced by different agents in the same cell type, an indicator might underreport caf_{free} values, especially high ones, and diminish, or even mask, differences [53,56]. On the other hand, an indicator may report a similar change in $[Ca^{2+}]_i$ as being different between two cells, if the compared cells feature different kS. This problem may be quite common, since intrinsic buffering capacity is known to differ between cell types [77,78] and may change with cell age [79-81]. To find out whether the observed $[Ca^{2+}]_i$ is affected by an indicator, it is enough to repeat the measurement with reduced indicator binding ratio (κd). If lowering the indicator concentration or affinity results in increasing indicator response, it is a clear sign that the $[Ca^{2+}]_i$ might be underestimated (Figures 1 & 7, Supplementary Figure 1). Unfortunately, such comparisons are rarely performed and indicator Ca^{2+} buffering and its potential implications do not receive as much attention as they deserve. Our own data suggest that fura-2 concentration in hippocampal neurons need to be much lower than 30-35 μM to report peak caf_o of 1 μM accurately (Figure 7). Some conservative estimates recommend values as low as 6-10 μM [40, 82], concentrations that performed well in our EGTA-buffered *in vitro* system (Figure 1, Supplementary Figure 1).

If lowering the indicator concentration is not feasible, the use of lower affinity indicators [9,48,51] may be an attractive option as they will be less likely to affect Ca^{2+} homeostasis (Fqn.14; Figure 3, Supplementary Figure 1C). If we assume that accurate determination of a [Ca^{2+}] of 1 μM can be accomplished with fura-2 concentration of 10 μM, the same can be achieved, at least in principle, with 12 μM fura-2FF (K_d=6 μM), 21 μM BTC (K_d =12 μM) or 40 μM mag-fura-2 (K_d=25 μM). However, as the indicator affinity decreases, so does the relative magnitude of the response (82% and 3.4% of the dynamic range of fura-2 and mag-fura-2, respectively), which limits usefulness to high Ca^{2+} concentrations (see also Supplementary Figure 1D). Interestingly, this is the range in which high affinity counterparts are most likely to fail (Figures 1 & 3, Supplementary Figures 1A & 1C). Despite this and other advantages [62], low affinity indicators have not gained much popularity and are rarely used.

As lowering indicator concentrations or affinity might not be feasible for practical reasons, and the formerly developed methods [21,63,76,77] may be too complex for routine experiment, we have developed a simplified approach to estimate indicator-independent free Ca^{2+} levels. Although conceptually similar to its predecessors [21,66,83,84], this procedure requires only data collected in almost any Ca^{2+} imaging experiment. To test it, we first processed data from well-defined *in vitro* systems (Figure 1) and found out that to work appropriately it requires data from at least two different caf_o (k≥2), collected with two or more indicator concentrations (i≥2) (Figure 4). Practically, this means that to obtain a minimal amount of data it is necessary, and possibly sufficient, to repeat the same experiment using two different fura-2 concentrations (Figure 4). Analysis of model data also shows that, while caf_o estimates are quite accurate, other parameters tend to deviate from the actual ones as the data scatter increases (Figure 5). As these trends are quite stable, it is possible to conclude that the actual valise are either lower (K_b) or higher (cat, buf) than those produced by the proposed method.

When applied to data collected in AM-loaded neurons, the tested procedure provided estimates of indicator-independent free Ca^{2+} concentration (caf_o) in resting and depolarized neutrons (Figures 7A & 7C) and offered insight into the nature of endogenous buffer properties (Figure 7B). As the data scatter affects these values in different ways (Figures 5-6), only the caf_o can be considered as reasonably accurate while the others, including buf, K_b and cat, constitute estimates of unknown accuracy. Although calculated buf (500-700 μM) and K_b (0.78-1.6 μM) (Figure 7B) are most likely under- or overestimated, they are consistent with the consensus notion that neurons contain large quantities of low affinity buffer. As the tested method also estimates total Ca^{2+} concentrations, subtracting the calculated values may provide a way to assess, albeit perhaps not very accurately (Figures 5C & 5D), the total calcium flux (Figure 7B).

It is interesting to note that mean caf_o calculated by averaging cafo in individual neurons containing the highest fura-2 concentration (dye~288 μM) before (34±4 nM) and after stimulation (1.76±0.38 μM) are much higher than caf_o derived from regression analysis of all data (22 nm and 1.08 μM, respectively (Figure 7C). These differences may result from inaccuracy of experimental data, but our *in vitro* experiments seem not to support this notion (Figure 5) Although we cannot rule this option out completely, there is ample, though indirect, evidence that excessive buffering might change the system behavior, increasing calcium influx by disrupting Ca^{2+} dependent inactivation of L-type voltage gated Ca^{2+} channels [85,86]. If fura-2 in high concentrations could do just that, it would create a paradoxical situation in which an indicator enhances Ca^{2+} influx (Figure 7C), yet masks the increase at the same time (Figure 7A). If this is confirmed to be the case, it would add to the growing list of indicator side effects [87] that includes inhibition of Na,K ATPase [88], activation of Ca^{2+} -activated K+ channels [89,90] and impairment of calcium release [91,92]. There is also no reason to think that the fluorescent BAPTA derivatives that are used as indicators act differently than BAPTA itself, which has been shown to reduce or even block neurotransmitter release [93,94], change neuron susceptibility to excitotoxicity [95,96] and impede cell differentiation [97].

It is clear that using the lowest possible indicator concentrations and replacing, when feasible, standard indicators such as fura-2 with low affinity analogues can minimize or even eliminate such unwanted effects. The same steps may also help to improve the accuracy of routine Ca^{2+} measurements. Should they prove insufficient, the indicator-independent free Ca^{2+} concentration, total Ca^{2+} influx and endogenous buffer properties can be estimated with the method we propose, using data collected in any AM ester loaded cells.

Conclusions

By binding calcium ions, fluorescent calcium indicators may markedly reduce their intracellular concentration and underreport $[Ca^{2+}]_i$. This problem may be theoretically solved by lowering indicator concentration to "safe" levels and/or using low affinity indicators. As these approaches may not always be feasible for practical reasons, extrapolating $[Ca^{2+}]_i$ to "no dye" conditions may prove useful in estimating the native, indicator-independent free Ca^{2+} concentration ([Ca^{2+}] o) even in AM ester loaded cells.

Acknowledgments

This study was supported by the Center for Investigation of Membrane Excitability Diseases (CIMED), the Hope Center for Neurological Disorders of Washington University and NIH grants P01 NS032636 and R01 NS36265 (to MPG). We are grateful to Ms. Ann Benz for providing the cells for this study and to Dr. C. McClenaghan and Ms. M. Hyrc for help in preparing the manuscript.

Conflict of Interest

None.

References

1. Brini M, Cali T, Ottolini D, Carafoli E (2014) Neuronal calcium signaling function and dysfunction. Cellular and molecular life sciences CMLS 71(15): 2787-2814.
2. Brini M, Carafoli E (2000) Calcium signalling a historical account recent developments and future perspectives. Cell MolLife Sci 57(3): 354-370.
3. Bootman MD, Collins TJ, Peppiatt CM, Prothero LS, MacKenzie L, et al. (2001) Calcium signalling an overview. Semin Cell Dev Biol 12(1): 3-10.
4. Petersen OH, Michalak M, Verkhratsky A (2005) Calcium signalling past present and future. Cell Calcium 38(3-4): 161-169.
5. Takahashi A, Camacho P, Lechleiter JD, Herman B (1999) Measurement of intracellular calcium. Physiol Rev 79(4): 1089-1125.
6. Williams DA, Bowser DN, Petrou S (1999) Confocal Ca^{2+} imaging of organelles, cells, tissues, and organs. Methods in enzymology 307: 441-469.
7. Demaurex N, Arnaudeau S, Opas M (2002) Measurement of intracellular Ca2+ concentration. Methods Cell Biol 70: 453-474.
8. Higley MJ, Sabatini BL (2008) Calcium signaling in dendrites and spines: practical and functional considerations. Neuron 59(6): 902-913.
9. Gee KR, Archer EA, Lapham LA, Leonard ME, Zhou ZL, et al. (2000) New ratiometric fluorescent calcium indicators with moderately attenuated binding affinities. Bioorg Med Chem Lett 10(14): 1515-1518.
10. Haugland RP (2002) Indicators for Ca^{2+}, Mg^{2+}, Zn^{2+} and other Metal ions. In: Haugland RP. Handbook of Fluorescent probes and Research Products. (9^{th} edition), Molecular Probes, Eugene, OR, USA, 767-817.
11. Paredes RM, Etzler JC, Watts LT, Zheng W, Lechleiter JD (2008) Chemical calcium indicators. Methods 46(3): 143-151.
12. Oheim M, vant Hoff M, Feltz A, Zamaleeva A, Mallet JM, et al. (2014) New red-fluorescent calcium indicators for optogenetics photoactivation and multi-color imaging. BBA 1843(10): 2284-2306.
13. Tsien RY (1980) New calcium indicators and buffers with high selectivity against magnesium and protons: design, synthesis, and properties of prototype structures. Biochemistry 19(11): 2396-2404.
14. Grynkiewicz G, Poenie M, Tsien RY (1985) A new generation of Ca^{2+} indicators with greatly improved fluorescence properties. J BiolChem. 260(6): 3440-3350.
15. Minta A, Kao JP, Tsien RY (1989) Fluorescent indicators for cytosolic calcium based on rhodamine and fluorescein chromophores. JBiolChem. 264(14): 8171-8178.
16. Adams SR (2010) How calcium indicators work. Cold Spring Harb Protoc 10(3): 1-5.
17. Neher E. (2008) Details of Ca2+ dynamics matter. J Physiol 586(8): 2031.
18. McMahon SM, Jackson MB (2018) An Inconvenient Truth: Calcium Sensors Are Calcium Buffers. Trends Neurosci 41(12): 880-884.
19. Tsien R, Pozzan T (1989) Measurement of Cytosolic Free Ca2+ with Quin2. Methods in Enzymology 172: 230-262.
20. Bers DM, Patton CW, Nuccitelli R (1994) A practical guide to the preparation of Ca2+ buffers. Methods Cell Biol 40: 3-29.
21. Neher E, Augustine GJ (1992) Calcium gradients and buffers in bovine chromaffin cells. J Physiol 450: 273-301.
22. Zhou Z, Neher E (1993) Mobile and immobile calcium buffers in bovine adrenal chromaffin cells. J Physiol 469: 245-273.
23. Neher E (1995) The use of fura-2 for estimating Ca buffers and Ca fluxes. Neuropharmacology. 34(11): 1423-1442.
24. Schwaller B (2010) Cytosolic Ca2+ buffers. Cold Spring Harb Perspect Biol 2(11): a004051.
25. Gilabert JA (2020) Cytoplasmic Calcium Buffering an Integrative Crosstalk. Adv Exp Med Biol 1131: 163-182.
26. Schwaller B (2020) Cytosolic Ca^{2+} Buffers Are Inherently Ca^{2+} Signal Modulators. Cold Spring Harb Perspect Biol 12(1): a035543.
27. Tsien RY, Pozzan T, Rink TJ (1982) Calcium homeostasis in intact lymphocytes: cytoplasmic free calcium monitored with a new, intracellularly trapped fluorescent indicator. JCell Biol 94(2): 325-334.
28. Rao GH, Peller JD, White JG (1985) Measurement of ionized calcium in blood platelets with a new generation calcium indicator. Biochem Biophys Res Commun 132(2): 652-657.
29. Moore ED, Becker PL, Fogarty KE, Williams DA, Fay FS (1990) Ca^{2+} imaging in single living cells: theoretical and practical issues. Cell Calcium 11(2-3): 157-179.
30. Tran NN, Leroy P, Bellucci L, Robert A, Nicolas A, et al. (1995) Intracellular concentrations of fura-2 and fura-2/am in vascular smooth muscle cells following perfusion loading of fura-2/am in arterial segments. Cell Calcium18(5): 420-428.
31. Dineley KE, Malaiyandi LM, Reynolds IJ (2002) A reevaluation of neuronal zinc measurements: artifacts associated with high intracellular dye concentration. MolPharmacol 62(3): 618-627.
32. Neher E (2013) Quantitative aspects of calcium fluorimetry. Cold Spring Harb Protoc 10: 918-924.
33. Fink C, Morgan F, Loew LM (1998) Intracellular fluorescent probe concentrations by confocal microscopy. Biophys J 75(4): 1648-1658.
34. Helm PJ, Patwardhan A, Manders EM (1997) A study of the precision of confocal, ratiometric, Fura-2-based [Ca^{2+}] measurements. Cell Calcium 22(4): 287-298.
35. Yasuda R, Nimchinsky EA, Scheuss V, Pologruto TA, Oertner TG, et al. (2004) Imaging calcium concentration dynamics in small neuronal compartments. Sci STKE 219: 1-19.
36. Ukhanov KY, Flores TM, Hsiao HS, Mohapatra P, Pitts CH, et al. (1995) Measurement of cytosolic Ca^{2+} concentration in Limulus ventral photoreceptors using fluorescent dyes. J Gen Physiol 105(1): 95-116.
37. Fierro L, Llano I (1996) High endogenous calcium buffering in Purkinje cells from rat cerebellar slices. J Physiol 496(Pt 3): 617-625.
38. Helmchen F, Imoto K, Sakmann B (1996) Ca^{2+} buffering and action potential-evoked Ca^{2+} signaling in dendrites of pyramidal neurons. Biophys J 70(2): 1069-1081.
39. Ali F, Kwan AC (2020) Interpreting in vivo calcium signals from neuronal cell bodies,axons, and dendrites: a review. Neurophotonics 7(1): 011402.
40. Tatsumi H, Katayama Y (1994) Calcium homeostasis in the presence of fura-2 in neurons dissociated from rat nucleus basalis theoretical and experimental analysis of chelating action of fura-2. J Neurosci Methods 53(2): 209-215.
41. Ashley RH (1986) Buffer capacity of intracellular Ca^{2+} indicators. Biochem J 240(1): 310-311.
42. Al Mohanna FA, Hallett MB (1988) The use of fura-2 to determine the relationship between cytoplasmic free Ca^{2+} and oxidase activation in rat neutrophils. Cell Calcium 9(1): 17-26.

43. Baylor SM, Hollingworth S (1988) Fura-2 calcium transients in frog skeletal muscle fibres. J Physiol 403: 151-92.

44. Hofer AM, Machen TE (1994) Direct measurement of free Ca in organelles of gastric epithelial cells. AmJPhysiol 267(3 Pt 1): G442-G451.

45. Rao GH, Peller JD, White JG (1985) Measurement of ionized calcium in blood platelets with a new generation calcium indicator. Biochem Biophys Res Commun 132(2): 652-657.

46. Nemeth EF, Scarpa A (1986) Cytosolic Ca^{2+} and the regulation of secretion in parathyroid cells. FEBS Lett 203(1): 15-19.

47. Nemeth EF, Scarpa A (1987) Rapid mobilization of cellular Ca^{2+} in bovine parathyroid cells evoked by extracellular divalent cations. Evidence for a cell surface calcium receptor. J Biol Chem 262(11): 5188-5196.

48. Iatridou H, Foukaraki E, Kuhn MA, Marcus EM, Haugland RP, et al. (1994) The development of a new family of intracellular calcium probes. Cell Calcium 15(2): 190-198.

49. Hyrc KL, Bownik JM, Goldberg MP (1998) Neuronal free calcium measurement using BTC/AM, a low affinity calcium indicator. Cell Calcium 24(3): 165-175.

50. Ito K, Miyashita Y, Kasai H (1997) Micromolar and submicromolar Ca^{2+} spikes regulating distinct cellular functions in pancreatic acinar cells. EMBO J 16(2): 242-251.

51. Raju B, Murphy E, Levy LA, Hall RD, London RE (1989) A fluorescent indicator for measuring cytosolic free magnesium. Am J Physiol. 256(3 Pt 1): C540-C548.

52. Hyrc KL, Bownik JM, Goldberg MP (2000) Ionic selectivity of low-affinity ratiometric calcium indicators: mag-Fura-2, Fura-2FF and BTC. Cell Calcium 27(2): 75-86.

53. Hyrc K, Handran SD, Rothman SM, Goldberg MP (1997) Ionized intracellular calcium concentration predicts excitotoxic neuronal death: observations with low-affinity fluorescent calcium indicators. JNeurosci 17(17): 6669-6677.

54. Carriedo SG, Yin HZ, Sensi SL, Weiss JH (1998) Rapid Ca^{2+} entry through Ca^{2+}-permeable AMPA/Kainate channels triggers marked intracellular Ca^{2+} rises and consequent oxygen radical production. J Neurosci 18(19): 7727-7738.

55. Keelan J, Vergun O, Duchen MR (1999) Excitotoxic mitochondrial depolarisation requires both calcium and nitric oxide in rat hippocampal neurons. JPhysiol 520 Pt 3(Pt 3): 797-813.

56. Stout AK, Reynolds IJ (1999) High-affinity calcium indicators underestimate increases in intracellular calcium concentrations associated with excitotoxic glutamate stimulations. Neuroscience 89(1): 91-100.

57. Regehr WG, Tank DW (1992) Calcium concentration dynamics produced by synaptic activation of CA1 hippocampal pyramidal cells. JNeurosci 12(11): 4202-4223.

58. Regehr WG, Atluri PP (1995) Calcium transients in cerebellar granule cell presynaptic terminals. Biophys J 68(5): 2156-2170.

59. Scheenen WJ, Makings LR, Gross LR, Pozzan T, Tsien RY (1996) Photodegradation of indo-1 and its effect on apparent Ca^{2+} concentrations. Chem-Biol 3(9): 765-774.

60. Kao S, Asanov AN, Oldham PB (1998) A Comparison of Fluorescence Inner-Filter Effects for Different Cell Configurations. Instrumentation Science & Technology 26(4): 375-387.

61. Hofer AM (2005) Measurement of free [Ca^{2+}] changes in agonist-sensitive internal stores using compartmentalized fluorescent indicators. Methods Mol Biol 312: 229-247.

62. Hyrc KL, Rzeszotnik Z, Kennedy BR, Goldberg MP (2007) Determining calcium concentration in heterogeneous model systems using multiple indicators. Cell Calcium 42(6): 576-589.

63. Berlin JR, Konishi M (1993) Ca^{2+} transients in cardiac myocytes measured with high and low affinity Ca^{2+} indicators. BiophysJ 65(4): 1632-1647.

64. Neher E, Augustine GJ (1992) Calcium gradients and buffers in bovine chromaffin cells. J Physiol 450: 273-301.

65. Oheim M, Naraghi M, Muller TH, Neher E (1998) Two dye two wavelength excitation calcium imaging: results from bovine adrenal chromaffin cells. Cell Calcium 24(1): 71-84.

66. Jackson MB, Redman SJ (2003) Calcium dynamics, buffering, and buffer saturation in the boutons of dentate granule-cell axons in the hilus. J Neurosci 23(5): 1612-1621.

67. Hyrc KL, Minta A, Escamilla PR, Chan PP, Meshik XA, et al. (2013) Synthesis and properties of Asante Calcium Red--a novel family of long excitation wavelength calcium indicators. Cell Calcium 54(4): 320-333.

68. Mennerick S, Que J, Benz A, Zorumski CF (1995) Passive and synaptic properties of hippocampal neurons grown in microcultures and in mass cultures. J Neurophysiol 73(1): 320-332.

69. Motulsky H, Christopoulos A (200) Fitting models to biological data using linear and nonlinear regression: a practical guide to curve fitting. Oxford University Press Oxford; New York: 104-108.

70. Schwaller B (2020) Cytosolic Ca^{2+} Buffers Are Inherently Ca^{2+} Signal Modulators. Cold Spring Harb Perspect Biol 12(1): 1- a035543.

71. Schwiening CJ, Thomas RC (1996) Relationship between intracellular calcium and its muffling measured by calcium iontophoresis in snail neurones. J Physiol 491(Pt 3): 621-633.

72. Xu T, Naraghi M, Kang H, Neher E (1997) Kinetic studies of Ca^{2+} binding and Ca^{2+} clearance in the cytosol of adrenal chromaffin cells. Biophys J 73(1): 532-545.

73. Aponte Y, Bischofberger J, Jonas P (2008) Efficient Ca^{2+} buffering in fast-spiking basket cells of rat hippocampus. J Physiol 586 (Pt 8): 2061-2075.

74. Helmchen F, Tank DW (2015) A single-compartment model of calcium dynamics in nerve terminals and dendrites. Cold Spring Harb Protoc 2015(2): 155-167.

75. Lin KH, Taschenberger H, Neher E (2017) Dynamics of volume-averaged intracellular Ca^{2+} in a rat CNS nerve terminal during single and repetitive voltage-clamp depolarizations. J Physiol 595(10): 3219-3236.

76. Hamid E, Church E, Alford S (2019) Quantitation and Simulation of Single Action Potential-Evoked Ca^{2+} Signals in CA1 Pyramidal Neuron Presynaptic Terminals. eNeuro 6(5): 1-22.

77. Canepari M, Vogt K, Zecevic D (2008) Combining voltage and calcium imaging from neuronal dendrites. Cell Mol Neurobiol 28(8): 1079-1093.

78. Lips MB, Keller BU (1998) Endogenous calcium buffering in motoneurones of the nucleus hypoglossus from mouse. J Physiol 511(Pt 1): 105-117.

79. Murchison D, Griffith WH (1998) Increased calcium buffering in basal forebrain neurons during aging. J Neurophysiol 80(1): 350-364.

80. Armbrecht HJ, Boltz MA, Kumar VB, Flood JF, Morley JE (1999) Effect of age on calcium-dependent proteins in hippocampus of senescence-accelerated mice. Brain Res 842(2): 287-293.

81. Bu J, Sathyendra V, Nagykery N, Geula C (2003) Age-related changes in calbindin-D28k, calretinin, and parvalbumin-immunoreactive neurons in the human cerebral cortex. Exp Neurol 182(1): 220-231.

82. Timmerman MP, Ashley CC (1986) Fura-2 diffusion and its use as an indicator of transient free calcium changes in single striated muscle cells. FEBS Lett 209(1): 1-8.

83. Helmchen F, Borst JG, Sakmann B (1997) Calcium dynamics associated with a single action potential in a CNS presynaptic terminal.Biophys J 72(3): 1458-1471.

84. Naraghi M, Muller TH, Neher E (1998) Two-dimensional determination of the cellular Ca^{2+} binding in bovine chromaffin cells. Biophys J 75(4): 1635-1647.

85. Tekmen M, Gleason E (2010) Multiple Ca^{2+}-dependent mechanisms regulate L-type Ca^{2+} current in retinal amacrine cells.J Neurophysiol 104(4): 1849-1866.

86. Tang Q, Bangaru ML, Kostic S, Pan B, Wu HE, et al. (2012) Ca^{2+}-dependent regulation of Ca^{2+} currents in rat primary afferent neurons: role of CaMKII and the effect of injury. J Neurosci 32(34): 11737-11749.

87. Bootman MD, Allman S, Rietdorf K, Bultynck G (2018) Deleterious effects of calcium indicators within cells; an inconvenient truth. Cell Calcium 73: 82-87.

88. Smith NA, Kress BT, Lu Y, Chandler Militello D, Benraiss A,et al. (2018) Fluorescent Ca^{2+} indicators directly inhibit the Na,K-ATPase and disrupt cellular functions. Sci Signal 11(515).

89. Zhang L, Pennefather P, Velumian A, Tymianski M, Charlton M,et al. (1995) Potentiation of a slow Ca^{2+} -dependent K+ current by intracellular Ca^{2+} chelators in hippocampal CA1 neurons of rat brain slices. J Neurophysiol 74(6): 2225-2241.

90. Lancaster B, Batchelor AM (2000) Novel action of BAPTA series chelators on intrinsic K+ currents in rat hippocampal neurones. JPhysiol 522(Pt 2): 231-246.

91. Richardson A, Taylor CW (1993) Effects of Ca^{2+} chelators on purified inositol 1,4,5-trisphosphate (InsP3) receptors and InsP3-stimulated Ca^{2+} mobilization. J Biol Chem 268(16): 11528-11533.

92. Alonso MT, Barrero MJ, Michelena P, Carnicero E, Cuchillo I,et al. (1999) Ca^{2+} -induced Ca^{2+} release in chromaffin cells seen from inside the ER with targeted aequorin. JCell Biol 144(2): 241-254.

93. Adler EM, Augustine GJ, Duffy SN, Charlton MP (1991) Alien intracellular calcium chelators attenuate neurotransmitter release at the squid giant synapse. J Neurosci 11(6): 1496-1507.

94. Augustine GJ, Adler EM, Charlton MP, Hans M, Swandulla D, et al. (1992) Presynaptic calcium signals during neurotransmitter release: detection with fluorescent indicators and other calcium chelators. J Physiol Paris 86(1-3): 129-134.

95. Tymianski M, Charlton MP, Carlen PL,Tator CH (1994) Properties of neuroprotective cell-permeant Ca^{2+} chelators: effects on $[Ca^{2+}]$ i and glutamate neurotoxicity in vitro. JNeurophysiol 72(4): 1973-1992.

96. Abdel Hamid KM, Tymianski M (1997) Mechanisms and effects of intracellular calcium buffering on neuronal survival in organotypic hippocampal cultures exposed to anoxia/aglycemia or to excitotoxins. J Neurosci 17(10): 3538-3553.

97. Gu X, Spitzer NC (1997) Breaking the code: regulation of neuronal differentiation by spontaneous calcium transients. Dev Neurosci 19(1): 33-41.

ISSN: 2574-1241

DOI: 10.26717/BJSTR.2023.53.008398

Krzysztof L Hyrc. Biomed J Sci & Tech Res